Kerr effect anomaly in magnetic topological insulator superlattices

OPEN ACCESS
IOP Publishing
Nanotechnology

Nanotechnology **31** (2020) 434001 (6pp)
https://doi.org/10.1088/1361-6528/aba210

Kerr effect anomaly in magnetic topological insulator superlattices

Jieyi Liu[1,2], Angadjit Singh[2,3], Balati Kuerbanjiang[1], Crispin H W Barnes[2] and Thorsten Hesjedal[1]

[1] Clarendon Laboratory, Department of Physics, University of Oxford, Oxford, OX1 3PU, United Kingdom
[2] Cavendish Laboratory, University of Cambridge, J J Thomson Avenue, Cambridge, CB3 0HE, United Kingdom
[3] Department of Physics, Royal Holloway, University of London, Egham Hill, Egham, TW20 0EX, United Kingdom

E-mail: Jieyi.Liu@physics.ox.ac.uk and Thorsten.Hesjedal@physics.ox.ac.uk

Received 7 May 2020, revised 16 June 2020
Accepted for publication 2 July 2020
Published 3 August 2020

Abstract

We report the magneto-optical Kerr effect (MOKE) study of magnetic topological insulator superlattice films with alternating transition-metal and rare-earth doping. We observe an unexpected hump in the MOKE hysteresis loops upon magnetization reversal at low temperatures, reminiscent of the topological Hall effect (THE) reported in transport measurements. The THE is commonly associated with the existence of magnetic skyrmions, i.e. chiral spin textures originating from topological defects in real space. Here, the observation of the effect is tied to ferromagnetic ordering in the rare-earth-doped layers of the superlattice. Our study may provide a new approach for the non-invasive optical investigation of skyrmions in magnetic films, complementary to electrical transport measurements, where the topological Hall signal is often the only hint of non-trivial magnetization patterns.

Keywords: topological insulator, magneto-optical Kerr effect, magnetic skyrmion, magnetic superlattice, topological Hall effect

(Some figures may appear in color only in the online journal)

1. Introduction

Topological insulators (TIs) are materials with a non-trivial band topology in momentum space, which is rooted in their strong spin–orbit coupling [1]. Magnetic doping or proximity coupling can break time-reversal symmetry in TIs and induce a gap in the linearly dispersed surface bands [2], leading to exotic transport phenomena such as the quantum anomalous Hall effect (QAHE) with chiral edge conduction [3]. Recently, another intriguing Hall effect, the so-called topological Hall effect (THE), has been simultaneously observed with the QAHE in Cr:$(Bi,Sb)_2Te_3$/$(Bi,Sb)_2Te_3$ TI heterostructures [4]. In fact, the THE has been experimentally confirmed in a number of magnetic TI (MTI) systems independent of the presence of the QAHE [5–7]. Revealing itself as an additional hump in the Hall resistance, the THE is a transport signature of non-trivial spin textures such as magnetic skyrmions [8, 9].

Magnetic skyrmions are small whirls with concentrically gradually canting spins, which can be regarded as pseudo-particles originating from topological defects in real space [10]. Skyrmions can be as small as several nanometres in size and can be easily created, manipulated and annihilated, making them ideal candidates for racetrack memories [11], radio-frequency devices [12], logic gate devices [13], and magnonic crystal applications [14], to name a few. The occurrence of the THE is strongly tied to the presence of skyrmions, which provide an emergent magnetic field [8, 15]. The THE is therefore a selective and unique way for detecting skyrmions

in magneto-conductance experiments [16]. However, recent studies suggested that the inverse conclusion is not necessarily true, i.e. that the presence of the THE is a guarantee for the presence of topologically non-trivial magnetic skyrmions [17–20]. Also in case of TIs, several experimental studies have cast doubt on whether the observed THE signal is indeed due to skyrmions [21–23]. Instead, it is plausible that if different parts of a thin film system, e.g. the surface and bulk, have different coercivities and temperature dependences, then the combined hysteresis loop can have humps mimicking the THE signal observed, e.g. in the prototypical skyrmion system MnSi [8]. Although this argument does not conclusively rule out the presence of skyrmions, it certainly highlights the demand for complementary techniques that are able to unambiguously confirm skyrmion phases in magnetic materials, such as resonant soft x-ray scattering and magnetic force microscopy [9, 24–27].

Here, we report the magneto-optical Kerr effect (MOKE) study of an MTI superlattice system with alternating transition-metal and rare-earth doping, i.e. [Cr:Sb_2Te_3 (CST)/ Dy:Bi_2Te_3 (DBT)]$_5$. We observe an extra hump feature in the MOKE signal of the superlattice at low temperatures, reminiscent of the THE observed in transport measurements, which may be attributed to the occurrence of magnetic skyrmions. Our work demonstrates that MOKE magnetometry may be an alternative method to probe skyrmions in magnetic heterostructures, providing a new route to the exploration of Dirac band materials with real-space spin topology.

2. Experimental

The TI superlattices were grown by molecular beam epitaxy (MBE) in a Createc system with a base pressure of $< 1 \times 10^{-10}$ Torr. For the growth of the [CST/DBT]$_5$ structure on *c*-plane sapphire substrates, a standard recipe was used [28], starting with a 3-nm-thick Bi_2Te_3 seed layer. After its deposition at 250 °C, the film was annealed at 300 °C under Te flux, before the CST and DBT layers were alternately grown at 300 °C. The nominal composition of the superlattice is [$Cr_{0.41}Sb_{1.59}Te_3$ (4 nm)/ $Dy_{0.62}Bi_{1.38}Te_3$ (4 nm)]$_5$. The superlattice was capped with an amorphous Bi layer. Reflection high-energy electron diffraction (RHEED) was used to monitor the growth *in situ*. The structural properties of the film were characterized *ex situ* using X-ray diffraction (XRD).

Polar MOKE magnetometry was used to investigate the magnetic properties of the superlattices. A stand-alone MOKE probe was mounted in a continuous-flow ^{4}He cryostat, using a continuous-wave diode laser with a wavelength of 850 nm and a Glan–Taylor polariser. The laser beam was further focused onto the sample, achieving a minimum spot size of 2.2 μm in diameter. The reflected light was modulated at 100 kHz using a photoelastic modulator, before going through the second polariser and finally reaching the photodetector. The Kerr angle is then given by the ratio between the AC (at 100 kHz) and DC photovoltages generated at the detector. For details of our setup we refer to reference [29].

Magneto-transport experiments were carried out on Hall bar devices measuring 1000 μm × 100 μm. They were fabricated out of the superlattice films using standard optical lithography and subsequent Ar^+ ion milling. Ohmic contacts were achieved using thermal evaporation and lift-off of Ti/Au films. The Hall bar devices were then secured in leadless chip carriers and electrically connected using wire bonding. The chip carriers were placed at the end of a transport measurement probe, which can also be loaded into the MOKE cryostat. The standard four-terminal AC lock-in technique was employed for the measurements, with an input current amplitude of 1 μA at a frequency of 77 Hz.

3. Results

Figure 1(a) shows a schematic of the TI superlattice. Five repeats of CST/DBT bilayers were grown on a Bi_2Te_3 seed layer on *c*-plane sapphire, and then terminated by a layer of amorphous Bi. The XRD spectrum of the TI superlattice displays the (00*l*) peaks of Sb_2Te_3 and Bi_2Te_3 layers without signs of secondary phases. These well-resolved (00*l*) peaks confirm the *c*-axis orientation and crystal structure of the superlattice. Figure 1(b) shows the XRD spectrum around the (00.15) and (00.18) film peaks, highlighting the superlattice properties. Throughout the growth, *in situ* RHEED shows clear streaks (figure 1(c)), indicating the growth is two-dimensional with smooth surfaces.

Figure 2 shows the temperature-dependent polar MOKE results for the TI superlattice. The measurement geometry is depicted in figure 2(a), where a magnetic field is applied perpendicular to the film plane. A linearly polarized laser beam at normal incidence is focused on the film and reflected with a small rotation angle (θ_K) in polarization. Figure 2(b) shows the magnetic hysteresis loops of the superlattice with the down-sweep and up-sweep curves marked in blue and red, respectively. The square shape of the loops confirms the ferromagnetic order of the material with its easy axis oriented out-of-plane. Strikingly, below 20 K, an extra hump feature can be found immediately after the magnetization reversal, which mimics the THE observed in magneto-transport experiments of various TI heterostructures [4–7]. To quantitatively track this feature in the hysteresis loops, we plot the magnitude of the hump versus temperature as shown in figure 2(c). Clearly, the effect decreases linearly with increasing temperature, and disappears at 20–25 K. This transition temperature may be related to the ferromagnetic ordering of DBT layers [30]. Finally, the magnetization of the film also decreases with temperature and approaches zero at about 55–60 K (figure 2(d)), marking the Curie temperature (T_C) of the dominant CST phase in the superlattice.

Figure 3 shows the temperature-dependent anomalous Hall effect (AHE) loops obtained on the TI micro-device in an out-of-plane magnetic field, following the measurement geometry depicted in figure 3(a). The longitudinal resistance (R_{xx}) of the micro-device reveals a ferromagnetic transition at 56 K, indicated by the maximum in R_{xx} (figure 3(b)). This temperature aligns with the T_C confirmed by the MOKE measurements. Interestingly, a minimum in resistance is found at 21 K, suggesting another magnetic phase transition, most likely associated with the DBT layers [30]. Figure 3(c) shows

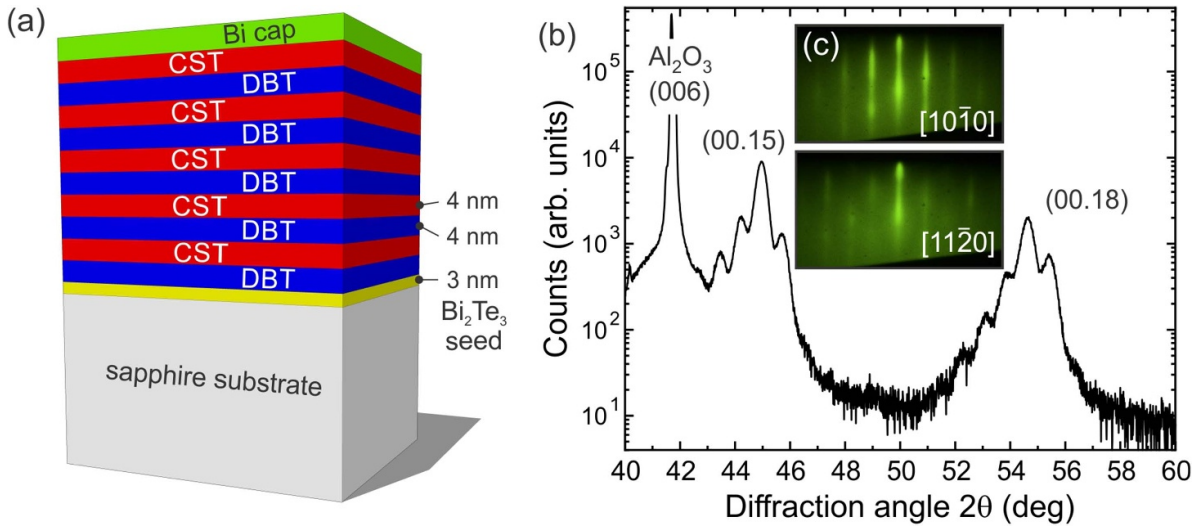

Figure 1. Structural characterization of the TI superlattice. (a) Schematic of the Cr:Sb_2Te_3 (CST)/Dy:Bi_2Te_3 (DBT)]$_5$ superlattice on a *c*-plane sapphire substrate. (b) X-ray diffraction data ($2\theta - \omega$ scan) for the CST/DBT superlattice on Al_2O_3 (0001), highlighting the superlattice peaks around the (00.15) and (00.18) film peaks. (c) Streaky RHEED patterns obtained from the CST surface at the end of the bilayer growth, along the [10$\bar{1}$0] and [11$\bar{2}$0] azimuths, respectively.

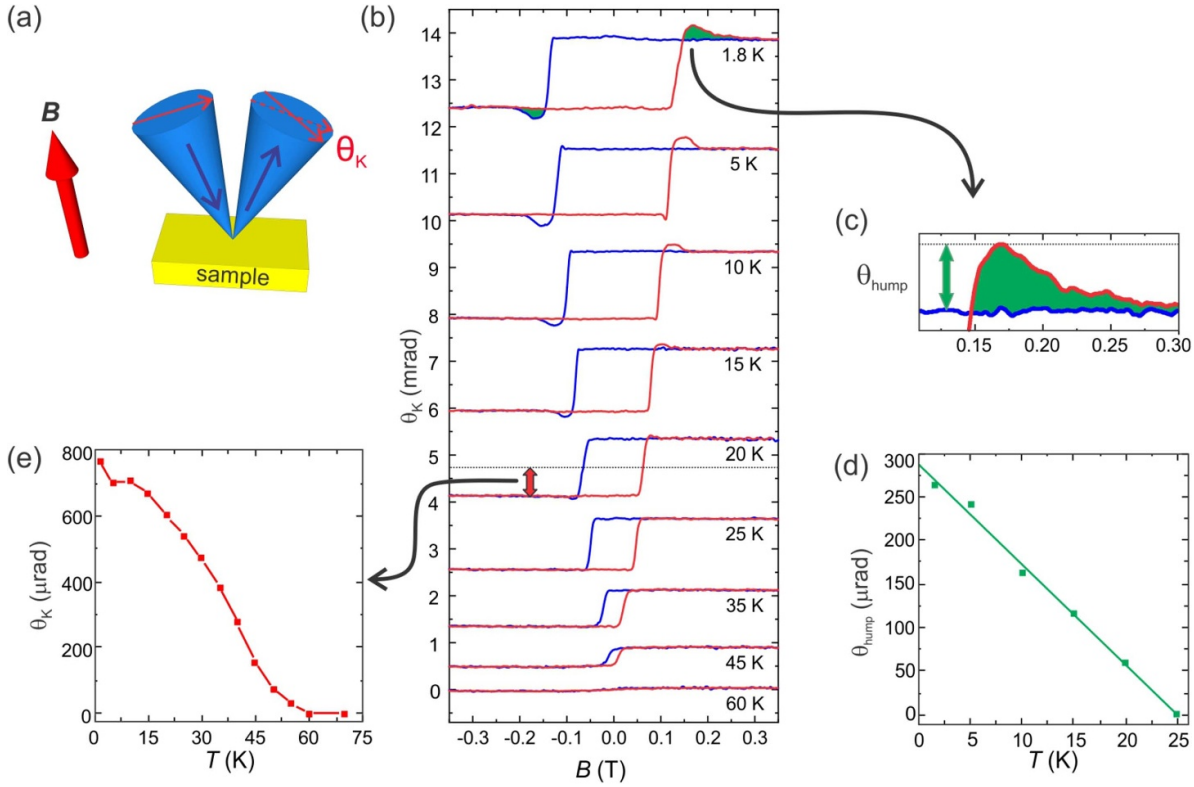

Figure 2. MOKE magnetometry results of the TI superlattice. (a) Measurement geometry of the polar MOKE experiment. (b) MOKE hysteresis loops for a range of temperatures between 1.8 and 60 K. The loops have been offset for clarity. The field plots obtained during down-sweeps are shown in blue and up-sweeps are in red, respectively. (c) Zoom-in image of the hump-like feature (illustrated by the shaded area in (a)), which is often referred to as the topological Hall signal in transport measurements. This feature is observed below 20 K. (d) Temperature dependence of the hump size, θ_{hump}, showing a linear decrease between 1.8 and 25 K. (e) Temperature dependence of the overall MOKE signal, θ_{K}. This signal vanishes above ∼60 K, indicating a phase transition of the whole film to a non-magnetic state.

the hysteresis loops of the Hall resistance (R_{xy}) as a function of magnetic field for selected temperatures. The down- and up-sweeps of the field are marked in blue and red, respectively. Note that at 45 K there is still a small, barely recognizable opening in the hysteresis loop. In contrast to the MOKE results, in which a hump appears right after magnetization reversals below 20 K, no such feature is found in the transport data across the entire temperature range. Finally,

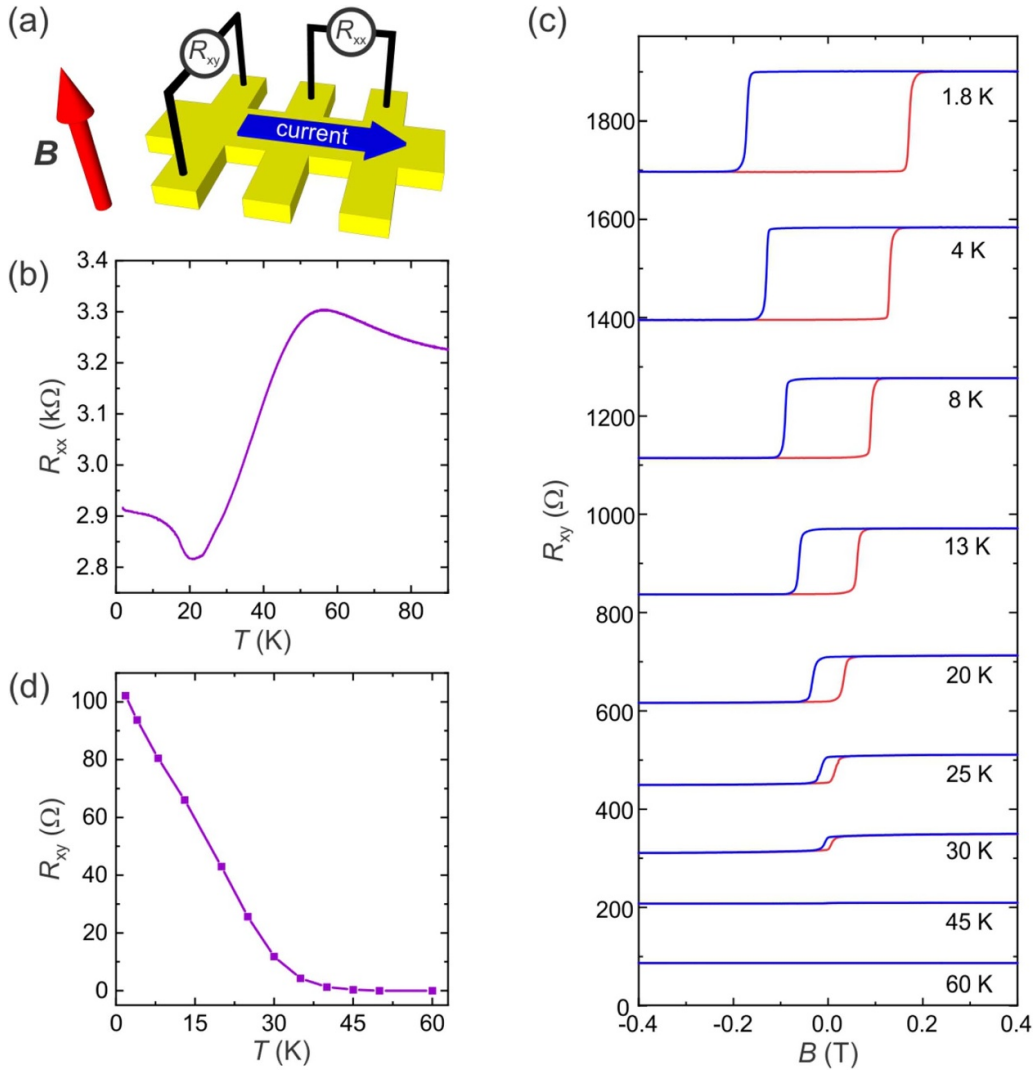

Figure 3. Magneto-transport results of the TI superlattice. (a) Hall bar measurement geometry with the field applied perpendicular to the superlattice. (b) Longitudinal resistance, R_{xx}, as a function of temperature. (c) Temperature-dependent anomalous Hall effect (AHE) loops for different temperatures from 1.8 to 60 K. The loops have been offset for clarity. The field plots obtained for the down-sweeps are shown in blue, and the opposite traces are in red. (d) Temperature dependence of the magnitude of the AHE signal.

figure 3(d) shows the monotonic decrease of the magnetization with increasing temperature. According to this graph, ferromagnetic order of the micro-device disappears at ∼45–50 K, slightly below the T_C extracted from the MOKE and longitudinal resistance measurements.

4. Discussion

In a previous study [30], we examined the magnetic properties of $[CST/DBT]_5$ films using element-specific X-ray circular magnetic dichroism (XMCD) at the Cr and Dy absorption edges, through which we confirmed ferromagnetic ordering in the DBT layers close to the interfaces with a Curie temperature of ∼17 K. This finding was supported by first-principles calculations that estimated a Curie temperature of 23 K in DBT, which was induced by proximity-coupling across DBT and CST interfaces. Here, in our transport experiments, this temperature is echoed by the minimum longitudinal resistance at 21 K. Furthermore, it is reasonable to assume that the appearance of humps in the MOKE loops below 20 K are tied to the presence of ferromagnetic ordering in the DBT layers.

Magnetic skyrmions, in which the spins are canted with respect to each other, rely on the appearance of the Dzyaloshinskii-Moriya interaction (DMI) which arises from strong spin–orbit coupling. MTIs are no strangers to skyrmions, and in fact, composite skyrmions have been observed in MTI/ferromagnet heterostructures [31]. Further, in TI heterostructures, the coupling between Bi *p*-orbitals and Cr *d*-orbitals can significantly enhance the DMI [32]. This could be a route leading to skyrmions in $[CST/DBT]_5$ superlattices as well, with Bi and Cr atoms located closely to one another at the interfaces. In fact, a hump feature similar to the one reported here has also been seen in the magneto-optical response of ferromagnetic $SrRuO_3$ thin films [33]. Bartram *et al* interpreted the results on $SrRuO_3$ using a Landau theory analysis of magneto-elastic coupling, from which they claimed

that strain gradients in the film lead to DMI, and further to the formation of skyrmions. Eventually, the skyrmions result in a laser-frequency-dependent Kerr signal which is modulated by an effective Hund's coupling. Although the true origins of the exotic hysteresis features in $SrRuO_3$ are still under debate [18, 34–36], strain could be a reason we observe a skyrmion-related hump feature in $[CST/DBT]_5$ as well. The lattice mismatch between CST and DBT of 3% can result in a built-up of strain in the superlattice [37], changing its physical properties compared to single-layer films.

Given the lack of the independent confirmation of skyrmions in this material, e.g. through magnetic microscopy, it is important to consider alternative explanations of the observed MOKE feature. In general, hump-like features are known to exist in MOKE hysteresis loops, and they are caused by diffracted laser beams from nano-sized patterns such as magnetic gratings and circular Permalloy disks [38]. In such diffraction-MOKE (or D-MOKE) experiments, the array size of the sample is required to be within $\lambda/2 - 10\lambda$, where λ is the wavelength of the laser [39]. As a wavelength of 850 nm was used in our study, the occurrence of a D-MOKE signal would require lateral correlation lengths of 425 nm–8.5 μm from the structural features. The lowest required length of 425 nm is still larger than the typical size of quintuple-layer surface terraces of $<$100 nm, which are observed in magnetically doped Sb_2Te_3 films [28]. Further, depending on the growth recipe, rotational domains may measure some μm across and therefore lead to D-MOKE humps. However, the typical domain sizes of CST are less than 500 nm and it is therefore unlikely to expect a significant contribution from D-MOKE [28]. In fact, we have not seen a D-MOKE contribution in any DBT or CST single-layer films or heterostructures [29, 40]. More importantly, since the laser beam is probing the magnetic film at normal incidence, surface terraces in the lateral direction should not contribute to the D-MOKE signal.

Another possible explanation of the hump feature is the two-domain transport model for TI heterostructures. By combining magnetic layers which may have different coercivities and signs of the anomalous Hall signal in a single system, their respective contributions to the magnetic and transport properties can lead to enhancement or compensation effects. In fact, extra humps in the transverse overall resistance have been experimentally observed in TI heterostructure systems, and several research groups have attributed this phenomenon to the two-domain model [18, 21–23]. Analogously, it appears possible that the MOKE signal of the TI superlattice may also show a hump feature, due to an averaged response of the different layers (or different magnetic domains for that matter). However, in our case, the THE-like hump is not present in the electrical magneto-transport measurements. At this point it is important to remember that MOKE and electrical transport (done on a patterned Hall bar) are probing on different lateral length scales and over different depths. Whereas transport measurements probe the entire volume of the Hall bar (100 μm in width), in MOKE measurements the probed sample volume is reduced, due to the laser spot size of 2 μm in combination with the limited laser penetration depth, which makes MOKE surface-sensitive. Therefore, the hump feature measured in surface-sensitive MOKE may reflect the local or microscopic properties of the sample near the interface, which may not result in a THE-like signal in electrical Hall measurements. By relocating the laser spot, we have systematically probed several areas of unpatterned superlattice samples (measuring 4 mm $\times$ 4 mm), which consistently show the same Kerr hump feature, indicating a good lateral uniformity of the sample. It is therefore unlikely that the same compensating two-domain effect is governing the measured MOKE response.

5. Conclusions

In conclusion, we report the observation of an additional hump feature in MOKE measurements of the magnetic TI superlattice $[CST/DBT]_5$. Using XRD and RHEED, we confirm the high structural quality of the superlattice film. The hump feature persists up to 20 K, coinciding with the temperature of proximity-induced ferromagnetic ordering in DBT. The origin of the Kerr hump is consistent with the presence of skyrmions, which could be due to the emergence of a strain-enhanced DMI as observed in oxide thin films. Further magnetic microscopy work is needed to either confirm or disprove the existence of skyrmions by direct imaging in real space or reciprocal space. Our study highlights the possibility of topologically non-trivial spin configurations in magnetic TIs, promoting the development of dissipationless spintronics by utilizing the interplay of chiral spin textures in real space and chiral band topology in momentum space. We encourage theorists to look into the origins of this novel Kerr feature, either linking it to magnetic skyrmions or other effects that have not been considered.

Acknowledgments

The authors are indebted to Dr Liam B Duffy for help with the sample growth. J L and T H acknowledge financial support from EPSRC (Grant No. EP/M020517/1). A S acknowledges financial support from the SGPC Cambridge Commonwealth Trust and C H W B is grateful for financial support from EPSRC (Grant No. EP/J00412X/1). T H and B K acknowledge financial support from the John Fell Oxford University Press Research Fund, and thank the EPSRC for support under grant EP/N032128/1 (Skyrmionics: From Magnetic Excitations to Functioning Low-Energy Devices) and RCaH for their hospitality.

ORCID iDs

Jieyi Liu https://orcid.org/0000-0001-6588-5987
Angadjit Singh https://orcid.org/0000-0003-4922-4956
Balati Kuerbanjiang https://orcid.org/0000-0001-6446-8209
Crispin H W Barnes https://orcid.org/0000-0001-7337-7245
Thorsten Hesjedal https://orcid.org/0000-0001-7947-3692

References

[1] Hasan M Z and Kane C L 2010 Coll.: Topological insulators *Rev. Mod. Phys.* **82** 3045

[2] Chen Y L *et al* 2010 Massive Dirac fermion on the surface of a magnetically doped topological insulator *Science* **329** 659–62

[3] Chang C-Z *et al* 2013 Experimental observation of the quantum anomalous Hall effect in a magnetic topological insulator *Science* **340** 167–70

[4] Jiang J *et al* 2020 Concurrence of quantum anomalous Hall and THEs in magnetic topological insulator sandwich heterostructures *Nat. Mater.* **19** 732–7

[5] Yasuda K *et al* 2016 Geometric Hall effects in topological insulator heterostructures *Nat. Phys.* **12** 555–9

[6] Liu C, Zang Y, Ruan W, Gong Y, He K, Ma X, Xue Q-K and Wang Y 2017 Dimensional crossover-induced topological Hall effect in a magnetic topological insulator *Phys. Rev. Lett.* **119** 176809

[7] He Q L *et al* 2018 Exchange-biasing topological charges by antiferromagnetism *Nat. Commun.* **9** 2767

[8] Neubauer A, Pfleiderer C, Binz B, Rosch A, Ritz R, Niklowitz P G and Böni P 2009 Topological Hall effect in the A phase of MnSi *Phys. Rev. Lett.* **102** 186602

[9] Matsuno J, Ogawa N, Yasuda K, Kagawa F, Koshibae W, Nagaosa N, Tokura Y and Kawasaki M 2016 Interface-driven topological Hall effect in $SrRuO_3$-$SrIrO_3$ bilayer *Sci. Adv.* **2** e1600304

[10] Fert A, Reyren N and Cros V 2017 Magnetic skyrmions: Advances in physics and potential applications *Nat. Rev. Mater.* **2** 1–15

[11] Parkin S S P, Hayashi M and Thomas L 2008 Magnetic domain-wall racetrack memory *Science* **320** 190–4

[12] Carpentieri M, Tomasello R, Zivieri R and Finocchio G 2015 Topological, non-topological and instanton droplets driven by spin-transfer torque in materials with perpendicular magnetic anisotropy and Dzyaloshinskii–Moriya interaction *Sci. Rep.* **5** 16184

[13] Zhang X, Ezawa M and Zhou Y 2015 Magnetic skyrmion logic gates: Conversion, duplication and merging of skyrmions *Sci. Rep.* **5** 9400

[14] Ma F, Zhou Y, Braun H B and Lew W S 2015 Skyrmion-based dynamic magnonic crystal *Nano Lett.* **15** 4029–36

[15] Nagaosa N and Tokura Y 2013 Topological properties and dynamics of magnetic skyrmions *Nat. Nanotechnol.* **8** 899–911

[16] Raju M, Yagil A, Soumyanarayanan A, Tan A K C, Almoalem A, Ma F, Auslaender O M and Panagopoulos C 2019 The evolution of skyrmions in Ir/Fe/Co/Pt multilayers and their topological Hall signature *Nat. Commun.* **10** 696

[17] Gerber A 2018 Interpretation of experimental evidence of the topological Hall effect *Phys. Rev.* B **98** 214440

[18] Kan D, Moriyama T, Kobayashi K and Shimakawa Y 2018 Alternative to the topological interpretation of the transverse resistivity anomalies in $SrRuO_3$ *Phys. Rev.* B **98** 180408

[19] Zhang W, Balasubramanian B, Ullah A, Pahari R, Li X, Yue L, Valloppilly S R, Sokolov A, Skomski R and Sellmyer D J 2019 Comparative study of topological Hall effect and skyrmions in NiMnIn and NiMnGa *Appl. Phys. Lett.* **115** 172404

[20] Zhang S, Xia S, Cao Q, Wang D, Liu R and Du Y 2019 Observation of topological Hall effect in antiferromagnetic FeRh film *Appl. Phys. Lett.* **115** 022404

[21] Liu N, Teng J and Li Y 2018 Two-component anomalous Hall effect in a magnetically doped topological insulator *Nat. Commun.* **9** 1282

[22] Fijalkowski K M, Hartl M, Winnerlein M, Mandal P, Schreyeck S, Brunner K, Gould C and Molenkamp L W 2020 Coexistence of surface and bulk ferromagnetism mimics skyrmion Hall effect in a topological insulator *Phys. Rev.* X **10** 011012

[23] Chen P *et al* 2020 Tailoring the hybrid anomalous Hall response in engineered magnetic topological insulator heterostructures *Nano Lett.* **20** 1731–7

[24] Zhang S L, Bauer A, Berger H, Pfleiderer C, van der Laan G and Hesjedal T 2016 Resonant elastic x-ray scattering from the skyrmion lattice in Cu_2OSeO_3 *Phys. Rev.* B **93** 214420

[25] Zhang S, van der Laan G, Müller J, Heinen L, Garst M, Bauer A, Berger H, Pfleiderer C and Hesjedal T 2018 Reciprocal space tomography of 3D skyrmion lattice order in a chiral magnet *Proc. Natl. Acad. Sci. U.S.A* **115** 6386–91

[26] Meng K-Y *et al* 2019 Observation of nanoscale skyrmions in $SrIrO_3$/$SrRuO_3$ bilayers *Nano Lett.* **19** 3169–75

[27] Huang H, Lee S-J, Kim B, Sohn B, Kim C, Kao C-C and Lee J-S 2020 Detection of the chiral spin structure in ferromagnetic $SrRuO_3$ thin film Arxiv 2004.08092

[28] Collins-McIntyre L J *et al* 2016 Structural, electronic and magnetic investigation of magnetic ordering in MBE-grown $Cr_xSb_{2-x}Te_3$ thin films *EPL (Europhys. Lett.)* **115** 27006

[29] Liu J *et al* 2019 A low-temperature Kerr effect microscope for the simultaneous magneto-optic and magneto-transport study of magnetic topological insulators *Meas. Sci. Technol.* **30** 125201

[30] Duffy L B, Frisk A, Burn D M, Steinke N-J, Herrero-Martin J, Ernst A, van der Laan G and Hesjedal T 2018 Imposing long-range ferromagnetic order in rare-earth-doped magnetic topological-insulator heterostructures *Phys. Rev. Mater.* **2** 054201

[31] Zhang S, Kronast F, van der Laan G and Hesjedal T 2018 Real-space observation of skyrmionium in a ferromagnet-magnetic topological insulator heterostructure *Nano Lett.* **18** 1057–63

[32] Chen J *et al* 2019 Evidence for magnetic skyrmions at the interface of ferromagnet/topological-insulator heterostructures *Nano Lett.* **19** 6144–51

[33] Bartram F M *et al* 2019 Topological Kerr effect Arxiv 1908.08974

[34] Qin Q *et al* 2019 Emergence of topological Hall effect in a $SrRuO_3$ single layer *Adv. Mater.* **31** 1807008

[35] Wysocki L *et al* 2020 Electronic inhomogeneity influence on the anomalous Hall resistivity loops of $SrRuO_3$ epitaxially interfaced with 5*d* perovskites *ACS Omega* **5** 5824–33

[36] Li Z *et al* 2020 Reversible manipulation of the magnetic state in $SrRuO_3$ through electric-field controlled proton evolution *Nat. Commun.* **11** 184

[37] Yu Yavorsky B, Hinsche N F, Mertig I and Zahn P 2011 Electronic structure and transport anisotropy of Bi_2Te_3 and Sb_2Te_3 *Phys. Rev.* B **84** 165208

[38] Vavassori P *et al* 1999 Magnetic information in the light diffracted by a negative dot array of Fe. *Phys. Rev.* B 59 6337

[39] Grimsditch M and Vavassori P 2004 The diffracted magneto-optic Kerr effect: What does it tell you? *J. Phys. Condens. Matter* **16** R275–R294

[40] Singh A *et al* 2018 Systematic study of ferromagnetism in $Cr_xSb_{2-x}Te_3$ topological insulator thin films using electrical and optical techniques *Sci. Rep.* **8** 17024